Photonic Interference Cancellation for LiDAR Sensors

James Garofolo, Yang Qi, Taichu Shi, Gabriel Tian, and Ben Wu, *Member, IEEE*

***Abstract*— We propose a multi-input LiDAR receiver that is capable of cancelling optical interference in the physical layer. This system leverages a blind source separation (BSS) technique to generate de-mixing parameters that can be implemented using photonic analog circuitry to separate interference signals from incoming ToF LiDAR pulses in real time. The system is capable of removing wideband optical noise in the form of environmental interference, free-space optical communication signals, other LiDAR sensors, and adversarial LiDAR spoofing devices without appreciably affecting the throughput of the sensor.**

***Index Terms*— Blind source separation, free-space optical communication, interference cancellation, LiDAR.**

I. Introduction

LIGHT detection and Ranging (LiDAR) is a powerful technology for computer vision and the modeling of 3D space, associated with many emerging technologies like autonomous driving [1]. It uses the constant and measurable travel speed of light to generate collections of points in space, referred to as "point clouds," which can be used to infer the presence of different objects in said sample space. The most elegant and cost-effective way to take this measurement is to use short optical pulses, and measure the time between rising edges, which can be detected using a thresholding mechanism. This method of measuring distance is primarily referred to as time-of-flight (ToF) LiDAR. While this solution works well in an optically isolated environment, problems arise when the quality of the signal is corrupted by external optical interference. This interference can originate from the ambient electro-optical noise in the environment [2], the emerging presence of free-space optical (FSO) communication links [3], [4], other LiDAR sensors in the same environment [5], or even from adversarial actors intending to cause harm with the interference they introduce [6], [7]. The presence of this interference forces LiDAR manufacturers to increase their transmission power to provide an acceptable Signal-To-Interference Ratio (SIR) in exchange for more power draw and cost of manufacture. This trade-off limits the viability of LiDAR sensors in technologies for which they are otherwise very well-suited, and thus warrants exploration into methods of removing interference from LiDAR signals.

The current methods for mitigating the effects of interference on LiDAR signals tend to fall into one of three categories: pattern recognition, digital signal processing, and physical layer signal processing. Pattern recognition practices in LiDAR signal processing can create noise immunity by way of making a uniquely identifiable signal to use in place of a pulse, and then recognizing that signal amongst the interference that it is measured with [8]. While this does create a system that is more robust to noise, it does add latency to the system, and is still not immune to noise-related errors in measurement. It also does nothing to improve the sensor's vulnerability to adversarial attacks, which can be designed to mimic any LiDAR signal provided to them without any circuit reconstruction necessary [6]. With adversarial attacks left intact, the only action that can be taken to prevent their influence is to detect the data as adversarial and discard it [7]. Digital signal processing techniques focus more on removing noise from the signal of interest (SOI), by way of techniques like wavelet domain spatial filtering [9]. These techniques, while effective, tend to be computationally demanding, adding an amount of latency to the system that may be incompatible with real-time applications. Additionally, because digital signal processing techniques require the exact time-domain behavior of the processed signals to be captured, systems that leverage them are required to have analog-to-digital converters (ADC's) that adhere to the LiDAR signal's Nyquist sampling limit. This enforces a trade-off between system price and spatial resolution, as the precision of ToF LiDAR and RaDAR signals is proportional to their pulse width [10]. Physical layer signal processing aims to mitigate the shortcomings of its digital counterpart by implementing the denoising processes in analog rather than digital. The removal of the digitization delay and the increased speed of analog computation results in a negligible addition of latency over the noisy system, making the ideal choice for time sensitive applications like autonomous driving. Photonic analog circuitry is particularly effective for these applications, as it can support throughputs similar to that of optical fiber communication cable, and is versatile enough to handle a wide variety of tasks, as demonstrated by [11]. Despite this advantage, research on physical layer improvements to LiDAR systems has mostly focused on removing noise originating from the LiDAR system itself [2]. This is likely due to the difficulty of implementing more complex or time-dependent denoising techniques in analog.

Manuscript received 12 June 2023; revised 25 August 2023; accepted 13 September 2023. Date of publication 18 September 2023; date of current version 29 September 2023. This work was supported by the National Science Foundation (NSF) under Grant ECCS-2128608. *(Corresponding author: Ben Wu.)*

The authors are with the Department of Electrical and Computer Engineering, Rowan University, Glassboro, NJ 08028 USA (e-mail: wub@rowan.edu).

Color versions of one or more figures in this letter are available at https://doi.org/10.1109/LPT.2023.3316592.

Digital Object Identifier 10.1109/LPT.2023.3316592

Blind source separation is a method by which a multi-input, multi-output (MIMO) system can differentiate signals from one another without the need for time or frequency division multiplexing, and without any prior knowledge of the incoming signals' characteristics. This is commonly done by way of using the second and fourth order moments of the signals with respect to one another. This technique generates a de-mixing matrix, which can be multiplied by the received signal vector to recover the original signals as they were prior to combination. This method of de-mixing signals is especially elegant, as the linear transform that separates the signals can be easily implemented in the physical layer or built into an application-specific integrated circuit, as demonstrated by [12] and [13] respectively. This technique has been utilized heavily in the field of optical communications, as it adds next to no latency, and requires sampling of only a small portion of the mixed signals for the derivation of the de-mixing matrix in the case of static systems [3]. Additionally, because only statistical information about the signal amplitudes is used to calculate the de-mixing matrices, this technique can be done using sub-Nyquist sampling circuits. This enables cost-effective noise cancellation in frequency bands for which digital signal processing techniques would not be feasible [14].

In this letter, we propose a multi-input LiDAR receiver that is capable of removing interference signals from one another through the use of photonic BSS. The receiver uses a pair of spatially separated collimator lenses to generate a received signal vector out of the combination of the LiDAR pulses and all other optical signals. By spatially separating the lenses, the receiver increases the likelihood of separability of the incoming signals. The separation of the signals is implemented using a balanced photodetector and optical tunable attenuators and delays, adding virtually no latency to the measurement of distances while improving the SIR of the measurements drastically. This system is also compatible with sub-Nyquist sampling circuitry, removing the trade-off between spatial resolution and the cost of the LiDAR receiver. The organization and use case of the proposed system is illustrated in Fig. 1

II. Principle and System Setup

A. Principle: Photonic Blind Source Separation

The mixing of two signals in a MIMO system can be described as a linear transform that adds a scaled version of each of the sent signals together to create each of the received signals. More formally,

$$\begin{bmatrix} x_1 \\ x_2 \end{bmatrix} = \begin{bmatrix} a_{11} & a_{12} \\ a_{21} & a_{22} \end{bmatrix} \begin{bmatrix} s_1 \\ s_2 \end{bmatrix} \tag{1}$$

where x_1 and x_2 are received signals, s_1 and s_2 are transmitted signals, and the a parameters are functions with respect to frequency that describe the transmission coefficients of each signal in the system as it propagates toward one of the receiver ports. These parameters are often referred to in vector/matrix notation as $\mathbf{X}$, $\mathbf{S}$ and $\mathbf{A}$. The "de-mixing" of these signals in this model can then be simplified down to performing the inverse of this linear transform, or more formally,

$$\mathbf{S} = \mathbf{A}^{-1}\mathbf{X} \tag{2}$$

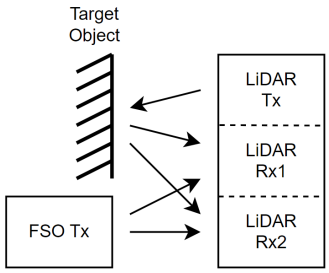

Fig. 1. Application scenario of the proposed system.

where the inverse matrix $\mathbf{A}^{-1}$ is known as the "de-mixing matrix" for the system. These matrices can be found using the second and fourth order moment of the received signals with respect to one another, as described in [12]. This yields the best results if the receivers are sufficiently spatially separated, such that $a_{11} \neq a_{21}$ and $a_{12} \neq a_{22}$. This strategy of statistical measurement is compatible with any two arbitrary signals, but ToF LiDAR signals are a special case that makes this procedure much easier. The following is a general equation for the inverse of a 2×2 matrix.

$$\begin{bmatrix} a_{11} & a_{12} \\ a_{21} & a_{22} \end{bmatrix}^{-1} = \frac{1}{a_{11}a_{22} - a_{21}a_{12}} \begin{bmatrix} a_{22} & -a_{12} \\ -a_{21} & a_{11} \end{bmatrix} \tag{3}$$

This form shows that a scaled version of s_1 can be recovered using only amplitude information about s_2, which can be measured directly while no LiDAR pulse is being transmitted. Because the sensor has control over the behavior of s_1 and the intent of this system is to discard s_2 after the statistical measurements are complete, measuring a_{12} and a_{12} is easily possible and sufficient to separate the desired signals without requiring any time-consuming statistical analysis. To de-mix the signals physically, one can simply align the two signals in time and implement the described de-mixing matrix somewhere along the signal path. This can easily be done with fiber-bound optical signals using tunable optical delays and attenuators without changing the throughput of the system at all.

B. Experimental Setup

Fig. 2 shows the experimental setup used to test this system. The LiDAR transmitter is made up of a Distributed Feedback (DFB) laser tuned to 1550nm, a polarization controller, Erbium-Doped Fiber Amplifier (EDFA), and an optical intensity modulator and a collimator lens that decouples the light from fiber. The intensity modulator is driven by a 3GHz Bit-Error Rate tester (BERT) that was configured to generate a pulse with a width of 0.33ns and a repetition rate of 3MHz to simulate a LiDAR sensor with a distance resolution of 48mm. The modulated light is decoupled at an optical power of 16.7dBm and directed towards a mirror that simulates the target object for the LiDAR sensor, and reflected back to the dual receiver for use in de-mixing. The interference generator is set up similarly, with the only change being the light source. For this experiment, a wideband laser was chosen to generate interference signals, in order to simulate the broad spectral contents of signals that tend to interfere with LiDAR sensors. The optical power of the interference transmitter was measured

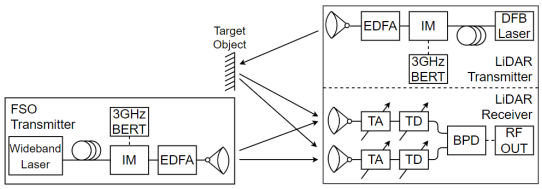

Fig. 2. System setup for testing the interference cancelling LiDAR receiver. (ASE: Amplified Spontaneous Emission source, BERT: Bit Error Rate Tester, IM: Intensity Modulator, EDFA; Erbium-Doped Fiber Amplifier, DFB: Distributed Feedback Laser, TA: Tunable Attenuator, TD: Tunable Delay, BPD: Bipolar Photodiode).

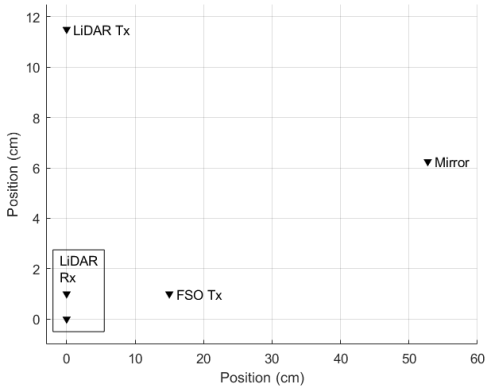

Fig. 3. Position of optical lenses and mirrors in the experimental setup.

to be 16.5dBm The dual receiver is made up of a pair of paths consisting of parallel collimator lenses, tunable attenuators, and tunable delays, terminating in one of the two inputs of a balanced photodetector. The tunable delays and attenuators in these paths can be controlled by the signal processing computer automatically, allowing for the implementation of one of the multiply-accumulate operations that make up the de-mixing transform. This enables the sensor to separate the LiDAR pulses from the interference signals before they are used to infer distance. The use of tunable attenuators to implement the transform coefficients also provides immunity to photodiode saturation by reducing saturation-level optical signals to a usable amplitude prior to analysis.

For the purposes of this analysis, the separation was computed in software. To do this, the collimator lenses and mirror in the setup were positioned with the spacings shown in Fig. 3. The one-way distance to the target is 53cm. The dual receiver ports were positioned close together and aimed parallel to one another, both to simulate the size constraints of building a sensor, as well as to ensure that drastically different optical powers are received by the reflection from the mirror. The result of this design decision is a mixing matrix that is easily separable via the statistical blind-source-separation system detailed in [12]. The rest of the positions in the diagram were fairly arbitrary.

In its correct position, Receiver 1 received -15.8dBm of optical power from the LiDAR transmitter and -17.8dBm from the interference transmitter. Receiver 2 received -21.8dBm from the LiDAR transmitter and -17.4dBm from the interference transmitter. Once the lenses were positioned, the receiver paths were replaced with photodetectors, and the transmission spectra of the four paths were measured over the

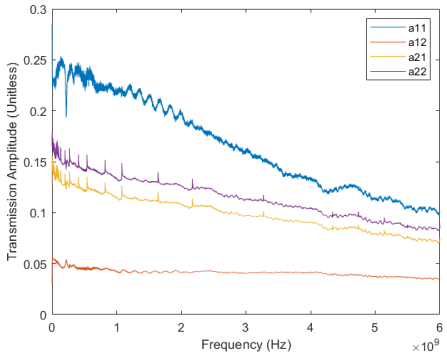

Fig. 4. Transmission spectrum for each channel.

bandwidth from DC to 6GHz with a precision of 3 significant figures. This would allow simulated data to be given a realistic frequency response that could be used to perform the simulated BSS system without the need to repeat experiments or change out equipment. These spectra could also be scaled as necessary in order to simulate different transmission distances and scenarios.

III. Simulated Results and Discussion

Measuring the four transmission paths resulted in the spectra shown in Fig. 4. This figure illustrates the distinct differences between each spectrum. While the interference signal spectra are similar in amplitude and shape, the LiDAR spectra are drastically different in amplitude due to the directionality of the parallel receivers. The interference signal spectra are also differently shaped from the LiDAR spectra, because of the difference in spectral contents of the laser sources used to carry the signals. These differences increase the likelihood of separability of the incoming signals.

To test the ability of the BSS system to de-noise the LiDAR signal, two different types of interference were tested. For the case of interference from wide-band LiDAR sensors, adversarial devices and/or free-space optical communication devices, a pseudo-random binary sequence (PRBS) was used to simulate interference. To ensure overlap of the signals' spectra, the bit rate of the PRBS signal needed to have a similar bit width to the pulse width of the LiDAR signal; however, the widths cannot be the same, or the two signals will be coherent and the separation of the signals will be trivial. To satisfy both of these conditions, the bit rate of the PRBS signal was chosen to be 2.9GBPS. Once the signals were sampled, they were rescaled with the spectra sampled from the system, put through the BSS system, and rescaled such that the peak amplitudes of the SOI and post-cancellation signal were the same. To demonstrate that this system is compatible with all types of LiDAR, the method proposed by [12] was used to compute the de-mixing transform rather than directly measuring the interference amplitudes. The resulting signals before and after separation are shown with the noisy signal in Fig. 5. This figure shows the signal after cancellation very closely resembling the ideal SOI. The comparison plot with the noisy signal shows that, while pulses could not be detected in the mixed signal using a threshold, they can easily be detected this way in the signal after cancellation. This separation was calculated to give an average interference rejection ratio of

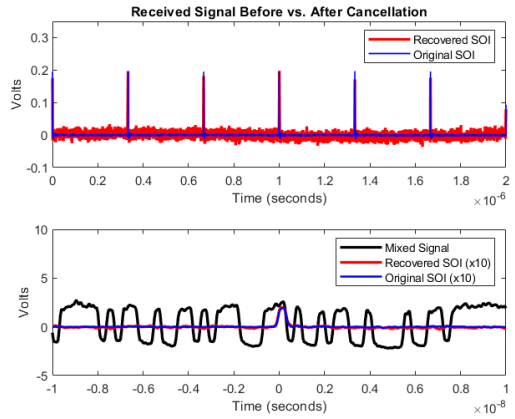

Fig. 5. Results of de-mixing with a PRBS interference signal. (a) Signal of interest before mixing and after de-mixing. (b) Original, mixed and de-mixed signals, with SOI's amplified by 10dB for visibility.

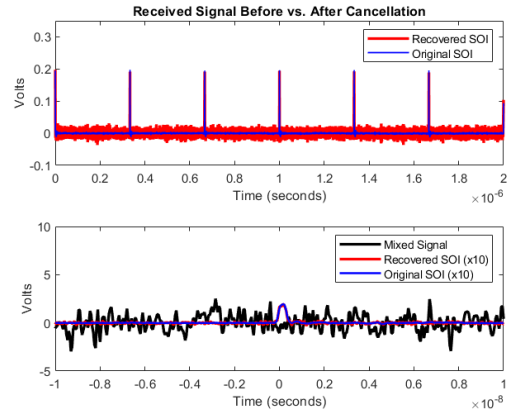

Fig. 6. Results of de-mixing with a Gaussian noise interference signal. (a) Signal of interest before mixing and after de-mixing. (b) Original, mixed and de-mixed signals, with SOI's amplified by 10dB for visibility.

41.7dBm, increasing the SIR by 46.5dB and resulting in a post-cancellation SIR of −2.7dB. Time jitter analysis shows that the distance measurement error caused by this residual interference is several orders of magnitude below the simulated precision of the sensor.

To test the case of environmental interference, a Gaussian distributed noise signal with a 20GHz sample rate was chosen as the interference signal, and the same test was repeated. The results of this test are shown in Fig. 6. As with the previous test, the signals were able to be separated sufficiently to allow for threshold detection of the LiDAR pulses. This separation yielded an average interference rejection ratio of 41.4dB, increasing the SIR by 42.4dB and resulting in a post-cancellation SIR of −2.4dB. This separation also yielded negligible distance measurement errors due to residual interference.

The interference rejection ratios of these separations are mainly limited by the frequency responses used to mix the signals. The BSS algorithm can only provide scalars for de-mixing coefficients, meaning that dissimilar mixing spectra for the same source signal will result in residual interference in the frequency components that cannot be perfectly matched. In physical implementations, noise will be accumulated that cannot be cancelled, further decreasing the maximum rejection ratio and corrupting measurements that could lead to more inaccurate de-mixing matrix estimation. These limitations scale in severity with the condition number of the mixing matrix, as demonstrated by [3], though this system is designed to minimize condition number as much as possible. Hardware experiments using this algorithm, such as the one detailed in [15], report achievable interference rejection ratios in the order of 30dB.

IV. Conclusion

We propose a multi-input LiDAR receiver that is capable of cancelling optical interference. This system uses blind source separation to remove interference signals from LiDAR pulses. The proposed system implements the interference cancellation calculations in photonic analog circuitry, meaning that the system does not appreciably reduce the sensor's throughput. This system was tested against wideband interference signals, simulating both digital and analog interference signals, and showing the potential to reject as much as 40dB of interference. This cancellation allows for threshold detection in scenarios where it would not be possible otherwise.

References

[1] J. Liu, Q. Sun, Z. Fan, and Y. Jia, "TOF LiDAR development in autonomous vehicle," in *Proc. IEEE 3rd Optoelectron. Global Conf. (OGC)*, Sep. 2018, pp. 185–190.

[2] F. Khoeini, B. Hadidian, K. Zhang, and E. Afshari, "A transimpedance-to-noise optimized analog front-end with high PSRR for pulsed ToF LiDAR receivers," *IEEE Trans. Circuits Syst. I, Reg. Papers*, vol. 68, no. 9, pp. 3642–3655, Sep. 2021.

[3] T. Shi, Y. Qi, and B. Wu, "Hybrid free space optical communication and radio frequency MIMO system for photonic interference separation," *IEEE Photon. Technol. Lett.*, vol. 34, no. 3, pp. 149–152, Feb. 1, 2022.

[4] H. Haas et al., "Introduction to indoor networking concepts and challenges in LiFi," *J. Opt. Commun. Netw.*, vol. 12, no. 2, pp. A190–A203, Feb. 2020.

[5] G. Kim, J. Eom, and Y. Park, "An experiment of mutual interference between automotive LiDAR scanners," in *Proc. 12th Int. Conf. Inf. Technol., New Generat.*, Apr. 2015, pp. 680–685.

[6] Y. Cao et al., "Adversarial sensor attack on LiDAR-based perception in autonomous driving," Aug. 2019, *arXiv:1907.06826*.

[7] K. M. A. Alheeti, A. Alzahrani, and D. Al Dosary, "LiDAR spoofing attack detection in autonomous vehicles," in *Proc. IEEE Int. Conf. Consum. Electron. (ICCE)*, Jan. 2022, pp. 1–2.

[8] Z.-J. Han, X. Tang, Z.-M. Wu, and G.-Q. Xia, "A real-time and anti-interference LiDAR based on field programmable gate array," in *Proc. 19th Int. Conf. Opt. Commun. Netw. (ICOCN)*, Aug. 2021, pp. 1–3.

[9] S. Yin and W. Wang, "LiDAR signal denoising based on wavelet domain spatial filtering," in *Proc. CIE Int. Conf. Radar*, Oct. 2006, pp. 1–3.

[10] M. A. Richards, J. A. Scheer, and W. A. Holm, *Principles of Modern Radar*, vol. 1. Rijeka, Croatia: SciTech, 2010.

[11] Q. Liu, B. Gily, and M. P. Fok, "Adaptive photonic microwave instantaneous frequency estimation using machine learning," *IEEE Photon. Technol. Lett.*, vol. 33, no. 24, pp. 1511–1514, Dec. 15, 2021.

[12] A. N. Tait et al., "Demonstration of multivariate photonics: Blind dimensionality reduction with integrated photonics," *J. Lightw. Technol.*, vol. 37, no. 24, pp. 5996–6006, Dec. 15, 2019.

[13] P. Y. Ma et al., "Blind source separation with integrated photonics and reduced dimensional statistics," *Opt. Lett.*, vol. 45, no. 23, p. 6494, 2020.

[14] T. Shi, Y. Qi, W. Zhang, P. Prucnal, J. Li, and B. Wu, "Sub-Nyquist optical pulse sampling for photonic blind source separation," *Opt. Exp.*, vol. 30, no. 11, pp. 19300–19310, 2022.

[15] Y. Qi, T. Shi, J. Garofolo, G. Tian, and B. Wu, "Wideband interference management for free space optical communication based on photonic signal processing," in *Proc. Frontiers Opt. Laser Sci. (FIO, LS)*, Washington, DC, USA: Optica Publishing Group, 2022, pp. 1–2. [Online]. Available: https://opg.optica.org/abstract.cfm?URI=FiO-2022-JTu4A.47